Electronic Supplementary Information

$NaYbF_4@CaF_2$ Core–Satellite Upconversion Nanoparticles: One-Pot Synthesis and Sensitive Detection of Glutathione

Bing Chen[a,b] *and Feng Wang**[,a,b]

[a]Department of Materials Science and Engineering, City University of Hong Kong, 83 Tat Chee Avenue, Hong Kong SAR, China

[b]City University of Hong Kong Shenzhen Research Institute, Shenzhen 518057, China

*Corresponding author. E-mail: fwang24@cityu.edu.hk

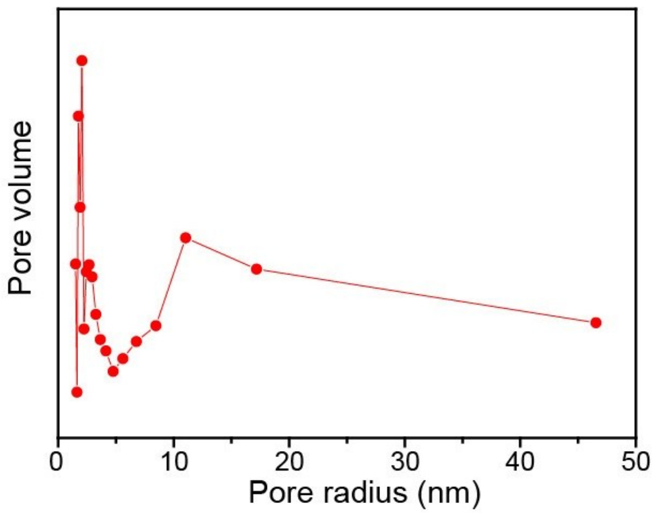

Figure S1. Barrette-Joynere-Halenda (BJH) pore-size distribution curve of the α-$NaYbF_4$@CaF_2 core–satellite nanoparticles.

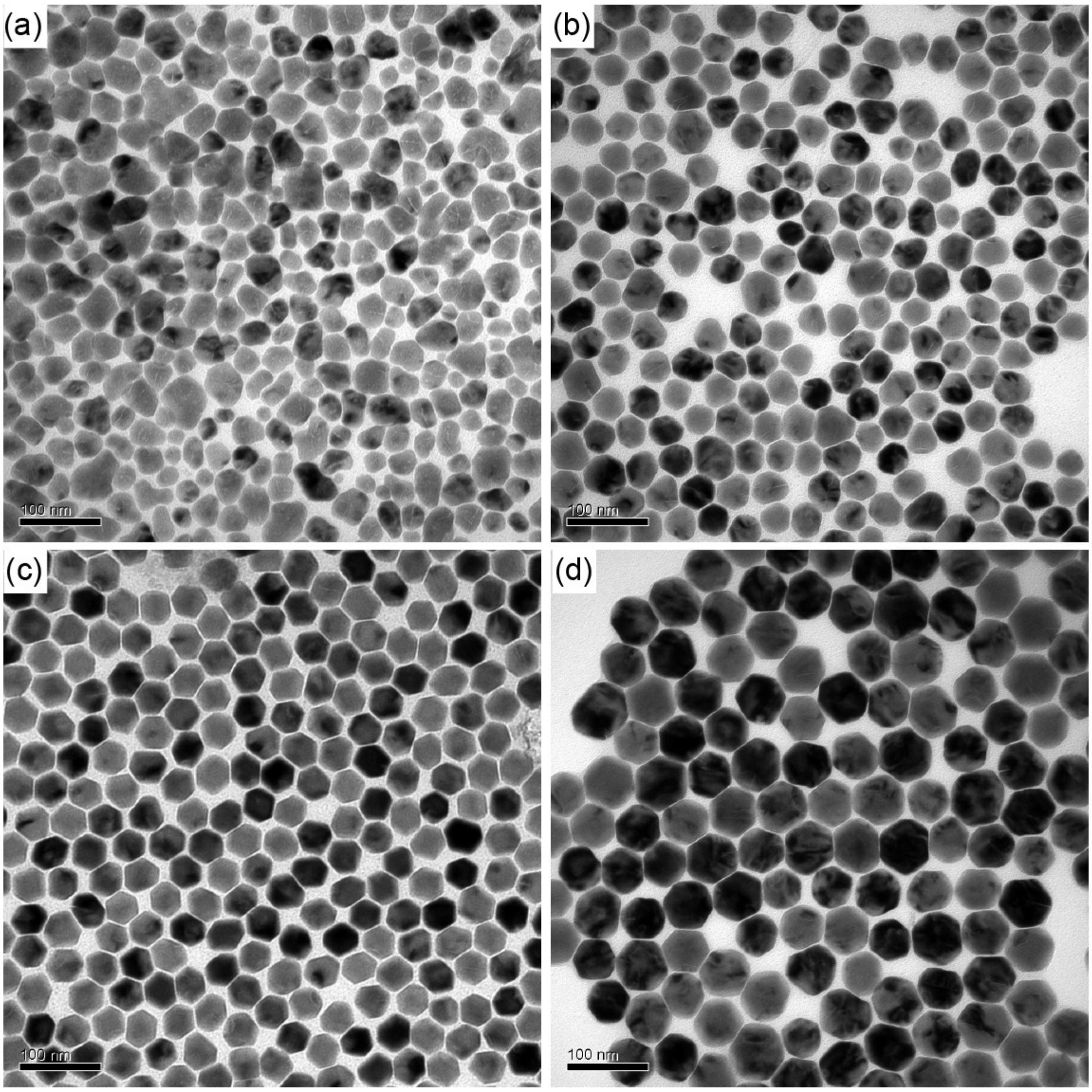

Figure S2. α-$NaYbF_4$ core nanoparticles synthesized by (a) one-shot quick injection (4 mL) and step-by-step injection at (b) 1.33 mL×3 times, (c) 1 mL×4 times, and (d) 0.8 mL×5 times.

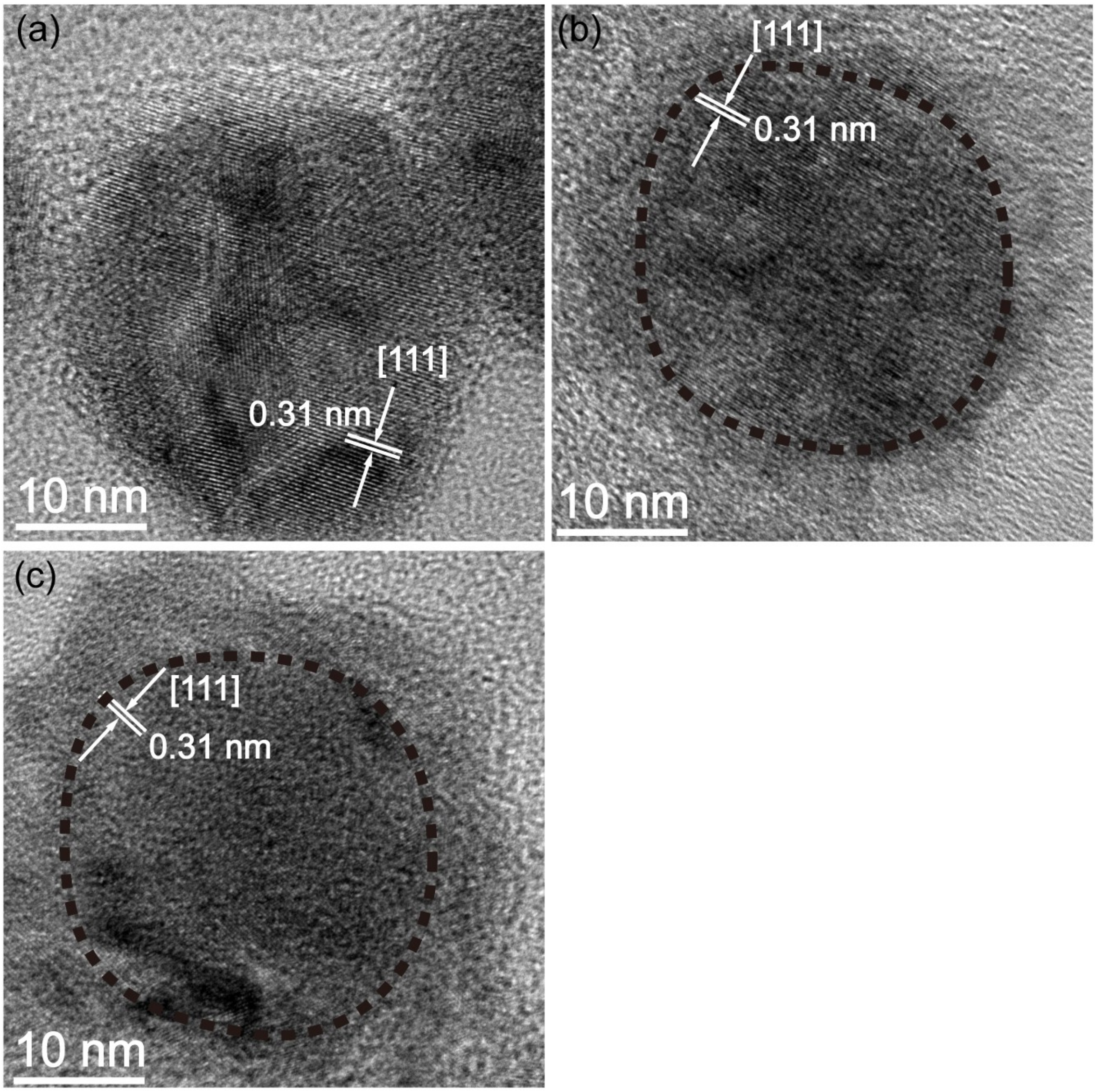

Figure S3. HRTEM images of the α-$NaYbF_4$@CaF_2 core–satellite nanoparticles (a) at the end of core reaction, (b) right after the first shell injection, and (c) at the end of the second shell reaction, respectively.

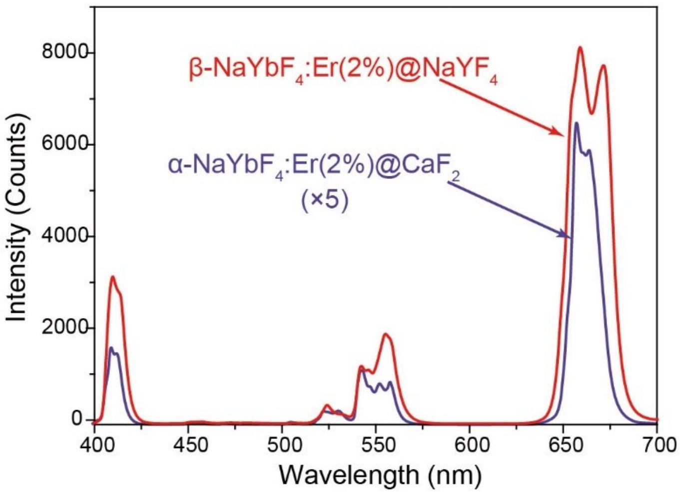

Figure S4. Comparison of upconversion performance of the α-$NaYbF_4$:Er (2%)@CaF_2 core–satellite nanoparticles and β-$NaYbF_4$:Er (2%)@$NaYF_4$ core–shell nanoparticles. The emission intensity of the α-$NaYbF_4$:Er (2%)@CaF_2 core–satellite nanoparticles is about one fifth the intensity of typical β-$NaYbF_4$:Er (2%)@$NaYF_4$ core–shell nanoparticles under the same testing condition.

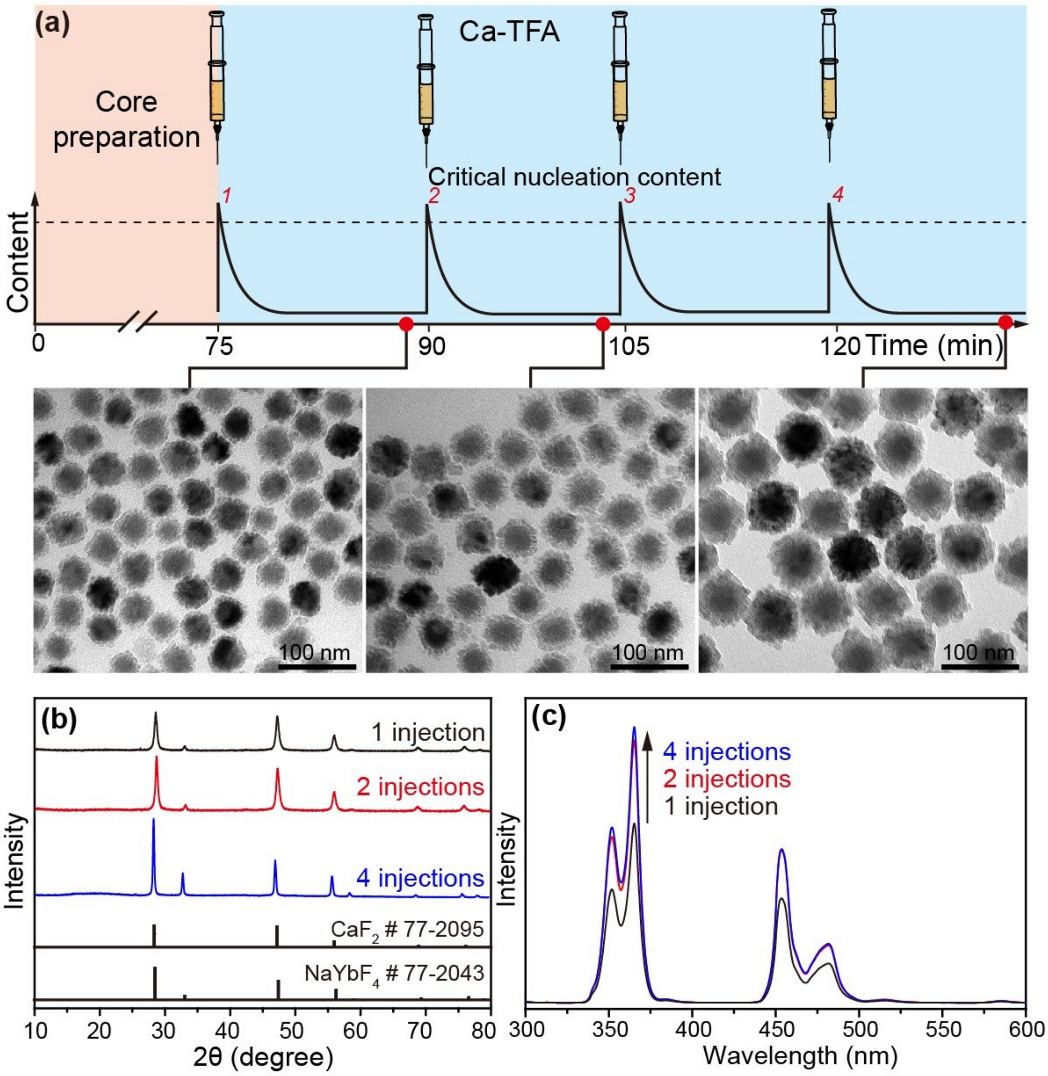

Figure S5. (a) Synthesis scheme and TEM images, (b) XRD pattern, and (c) photoluminescence spectra of the α-$NaYbF_4$:Tm (1%)@CaF_2 core–satellite UCNPs prepared by a step-by-step injection of excessive CaF_2 shell precursors (4 mL). The TEM images show a continuous enlargement in particle size as increasing precursor content. However, the comparison of PL spectra show that the emission intensity is unlikely to be further enhanced by growing a thick shell (4 injections of shell precursor).

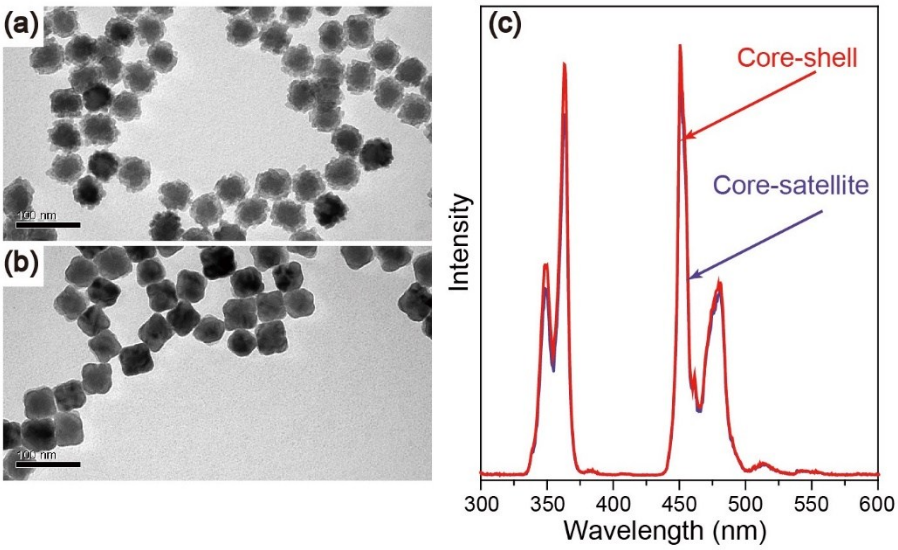

Figure S6. TEM images of (a) α-$NaYbF_4$:Tm (1%)@CaF_2 core–satellite nanoparticles and (b) α-$NaYbF_4$:Tm (1%)@CaF_2 core–shell nanoparticles after removal of oleate ligands by acidic treatment. (c) Upconversion spectra of the α-$NaYbF_4$:Tm (1%)@CaF_2 core–satellite nanoparticles and core–shell nanoparticles in aqueous solution. The results show that the satellite CaF_2 coatings provide equivalent protection of the upconversion core as dense shells in aqueous media.

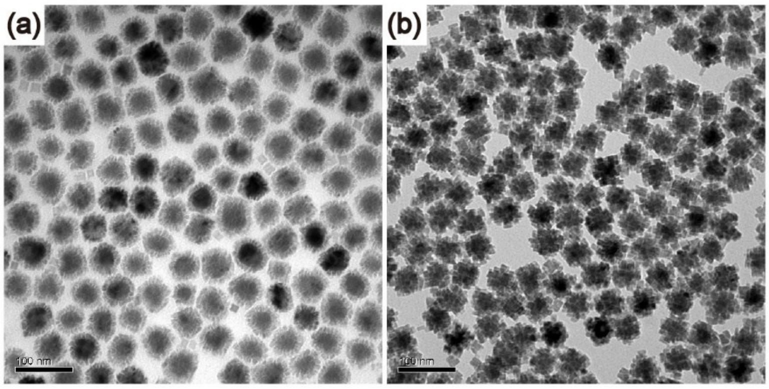

Figure S7. TEM images of (a) α-$NaYF_4$@CaF_2 core–satellite nanoparticles and (b) α-$NaYbF_4$@SrF_2 core–satellite nanoparticles.

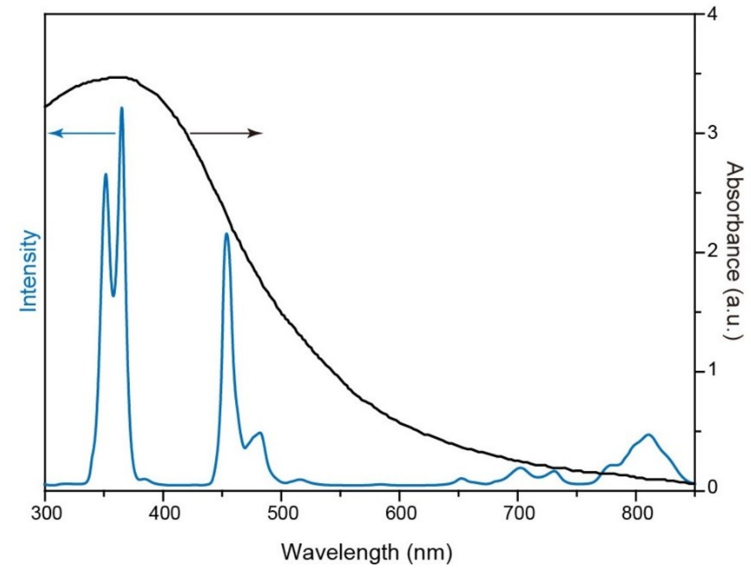

Figure S8. Absorption spectrum of MnO_2 showing the spectral overlapping with the emission spectrum of the α-$NaYbF_4$:Tm (1%)@CaF_2 UCNPs excited at 980 nm.

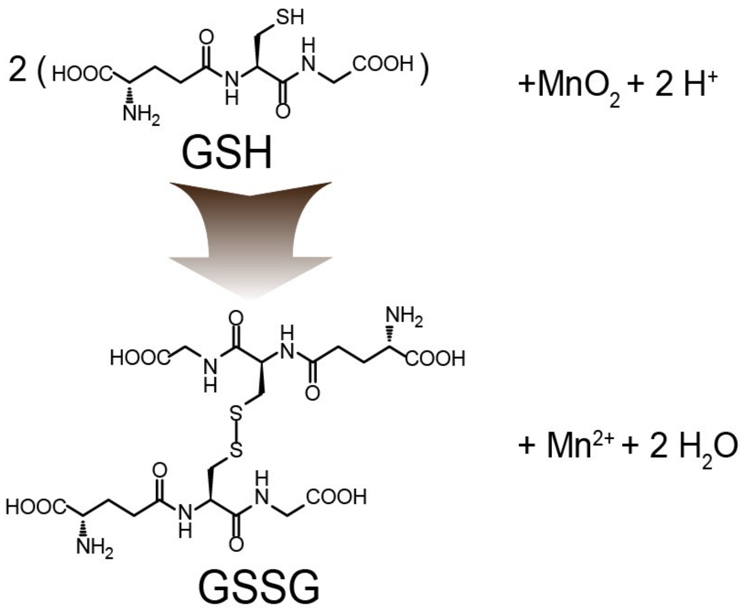

Figure S9. Basic reaction principle of GSH detection.

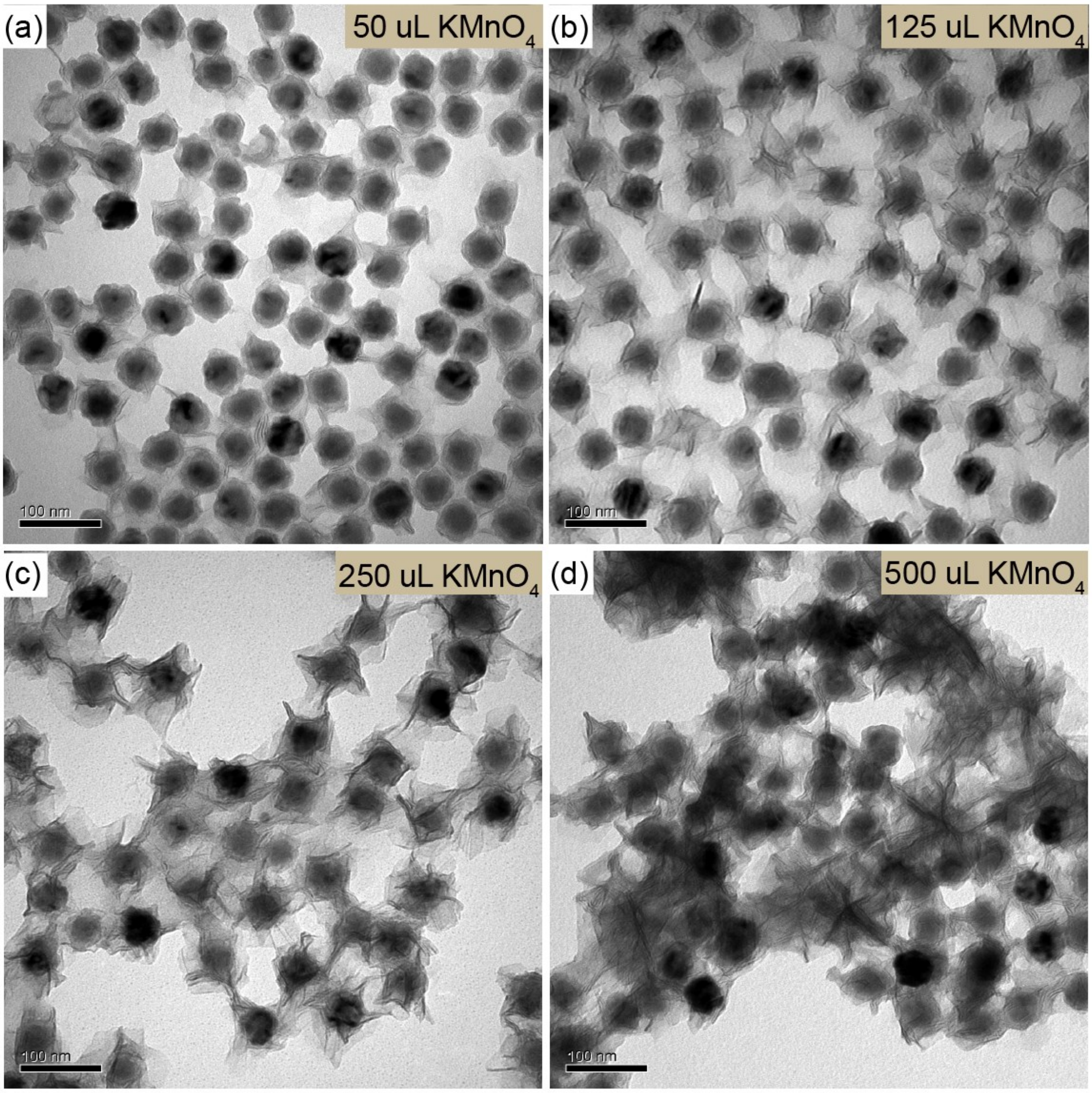

Figure S10. TEM images of the α-$NaYbF_4$:1%Tm@CaF_2@MnO_2 nanohybrids synthesized by mixing the α-$NaYbF_4$:Tm (1%)@CaF_2 core–satellite UCNPs with CTAB, MES, and different amount of $KMnO_4$ (50–500 μL, 10 mM) for 30 min.

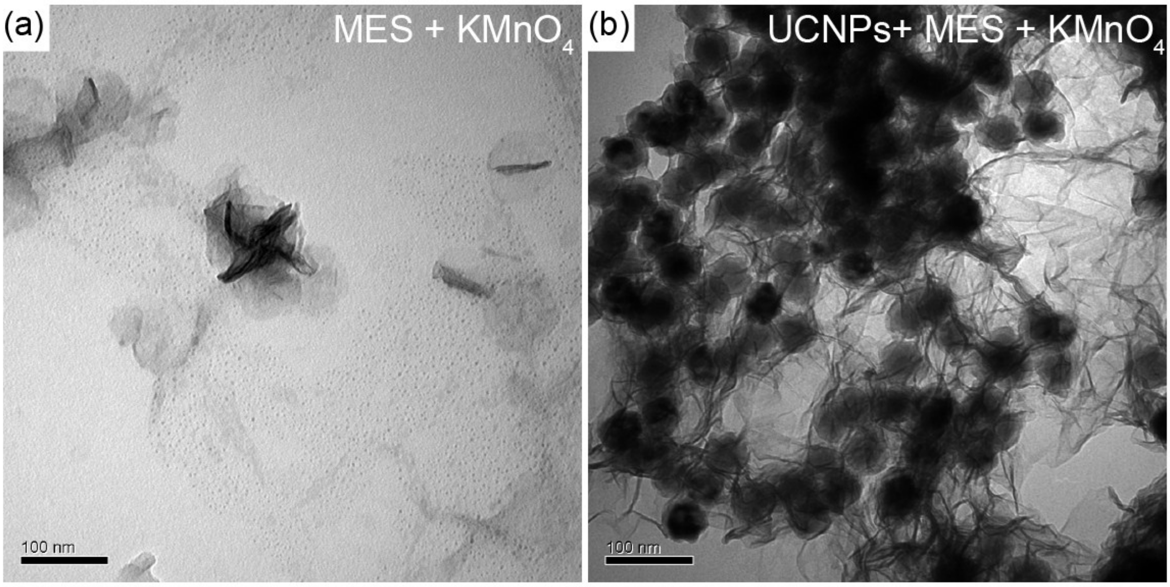

Figure S11. (a) TEM image of MnO_2 nanosheets synthesized by mixing of MES and $KMnO_4$ with ultrasound treatment and centrifugation for 30 min. (b) TEM image of UCNP + MnO_2 hybrids synthesized by mixing the α-$NaYbF_4$:Tm (1%)@CaF_2 core–satellite UCNPs, MES, and $KMnO_4$ with ultrasound treatment and centrifugation.

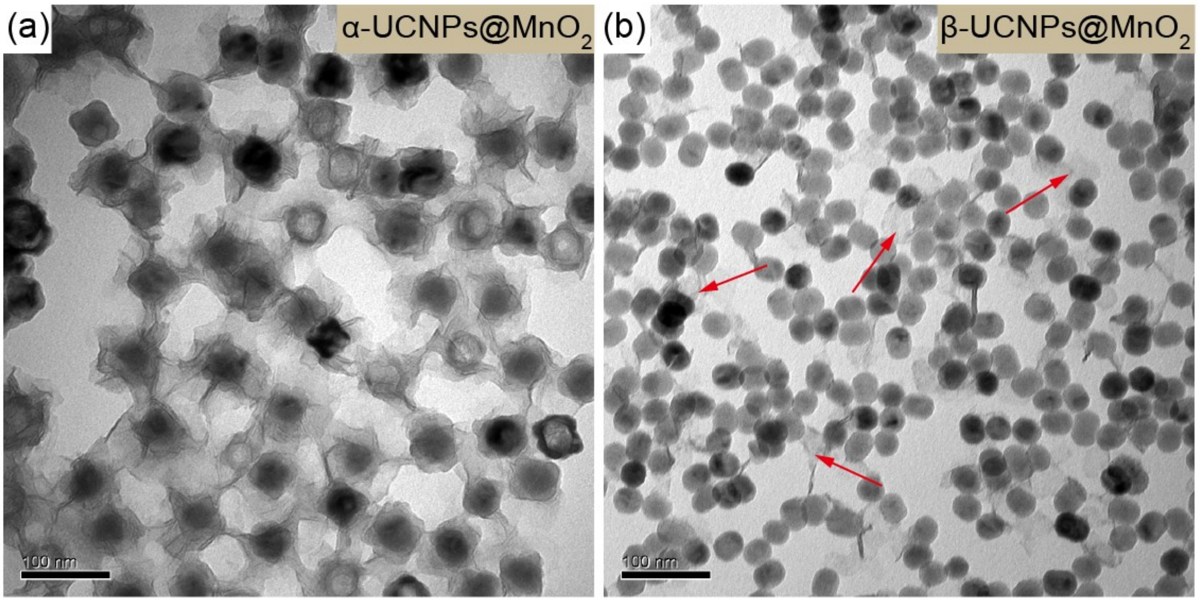

Figure S12. TEM images of UCNPs@MnO_2 hybrids using (a) α-$NaYbF_4$:Tm (1%)@CaF_2 core–dense shell UCNPs and (b) β-$NaYbF_4$:Tm (1%)@$NaYF_4$ UCNPs, respectively. Note that the layered MnO_2 in b is highlighted with red arrow.

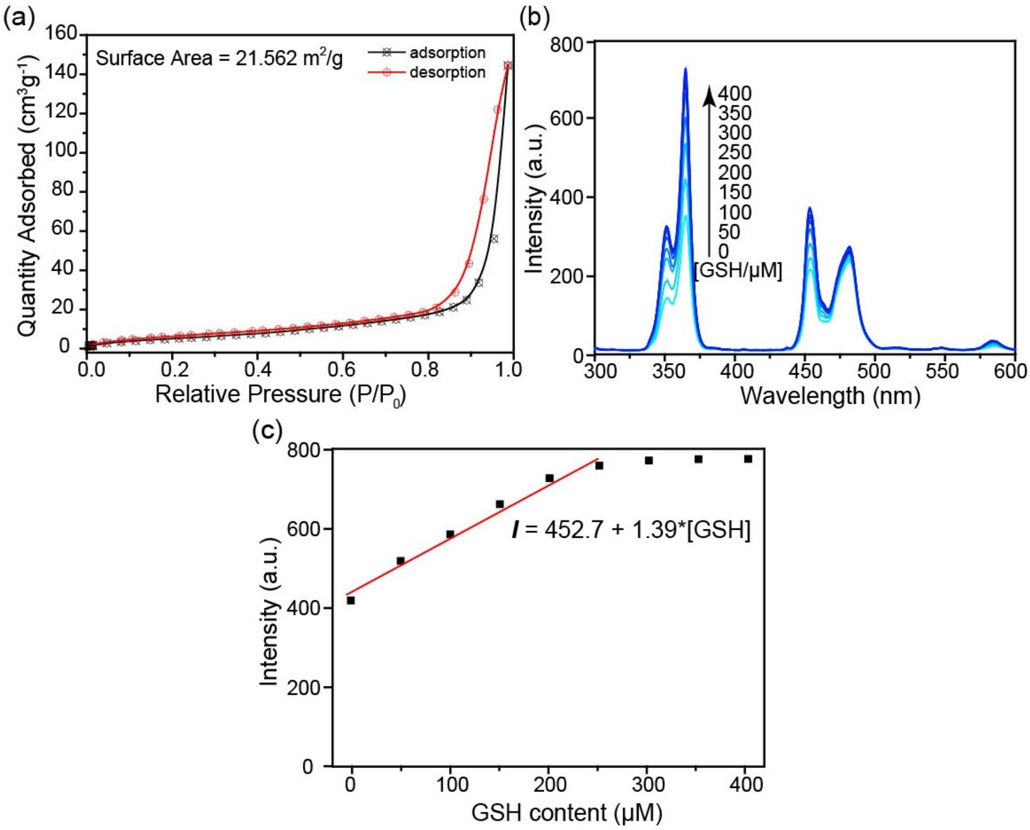

Figure S13. (a) Nitrogen adsorption-desorption isotherms of α-$NaYbF_4$:Tm (1%)@CaF_2 core–dense shell UCNPs. (b) Photoluminescence response of MnO_2-modified α-$NaYbF_4$:Tm (1%)@CaF_2 core–dense shell UCNPs as a function of GSH content. (c) Calibration curve of GSH detection using the MnO_2-modified α-$NaYbF_4$:Tm (1%)@CaF_2 core–dense shell nanohybrids. LOD = 0.88 μM.